Supporting Information for

High entropy stabilizing lattice oxygen participation of Ru-based oxides in acidic water oxidation

Yaodong Yu,[a] Hongdong Li,[a] Jiao Liu,[a] Wenxia Xu,[a] Dan Zhang,[b] Juan Xiong,[a] Bin Li,[c] A.O. Omelchuk,[d] Jianping Lai,[a] and Lei Wang*,[a,b]*

[a] State Key Laboratory Base of Eco-Chemical Engineering, International Science and Technology Cooperation Base of Eco-chemical Engineering and Green Manufacturing, College of Chemistry and Molecular Engineering, Qingdao University of Science and Technology, Qingdao 266042, P. R. China

[b] Shandong Engineering Research Center for Marine Environment Corrosion and Safety Protection, College of Environment and Safety Engineering, Qingdao University of Science and Technology, Qingdao 266042, P. R. China

[c] College of Materials Science and Engineering, Qingdao University of Science and Technology, Qingdao 266061, P. R. China

[d] V.I. Vernadskii Institute of General and Inorganic Chemistry of the Ukrainian NAS, prospekt Palladina 32/34, 03680 Kyiv, Ukraine

Chemicals: Molybdenumhexacarbonyl ($Mo(CO)_6$, 98%) and Nickel (II) acetylacetonate ($Ni(acac)_2$, 95%) were bought from Sigma-Aldrich. Chromium(III) acetylacetonate ($Cr(acac)_3$, 97%), Iron (III) 2,4-pentanedionate ($Fe(acac)_3$), Nafion solution (5 wt.%) were supplied by Alfa Aesar. Triruthenium

dodecacarbonyl ($Ru_3(CO)_{12}$, 98%) was purchased from Aladdin. Carbon nanotube, multi-walled (MWCNT) was bought from Aladdin.

Preparation of RuNiMoCrFeO$_x$/CNT. First, 8.0 mg $Ru_3(CO)_{12}$, 3.3 mg $Ni(acac)_2$, 3.3 mg $Mo(CO)_6$, 4.4 mg $Fe(acac)_3$, 2.8 mg $Cr(acac)_3$ and 9.0 mg of processed MWCNT were mixed and ground in a mortar for 10 minutes to mix evenly. The mixture was then placed in a 10 mL quartz bottle and heated in a household microwave oven at 1000 W starting at room temperature for 120 seconds. The black pellet product was collected by centrifugation and washed three times with ethanol. Finally, the black pellet product was dried in an oven at 60°C for 6 hours for further use.

Preparation of RuNiMoCrO$_x$/CNT. First, 8.0 mg $Ru_3(CO)_{12}$, 3.3 mg $Ni(acac)_2$, 3.3 mg $Mo(CO)_6$, 2.8 mg $Cr(acac)_3$ and 8.0 mg of processed MWCNT were mixed and ground in a mortar for 10 minutes to mix evenly. Other treatments are the same as RuNiMoCrFeO$_x$/CNT.

Preparation of RuMoCrFeO$_x$/CNT. First, 8.0 mg $Ru_3(CO)_{12}$, 3.3 mg $Mo(CO)_6$, 4.4 mg $Fe(acac)_3$, 2.8 mg $Cr(acac)_3$ and 8.0 mg of processed MWCNT were mixed and ground in a mortar for 10 minutes to mix evenly. Other treatments are the same as RuNiMoCrFeO$_x$/CNT.

Preparation of RuNiMoO$_x$/CNT. First, 8.0 mg $Ru_3(CO)_{12}$, 3.3 mg $Ni(acac)_2$, 3.3 mg $Mo(CO)_6$ and 7.0 mg of processed MWCNT were mixed and ground in a mortar for 10 minutes to mix evenly. Other treatments are the same as RuNiMoCrFeO$_x$/CNT.

Preparation of RuNiCrO$_x$/CNT. First, 8.0 mg $Ru_3(CO)_{12}$, 3.3 mg $Ni(acac)_2$, 2.8 mg $Cr(CO)_6$ and 6.0 mg

of processed MWCNT were mixed and ground in a mortar for 10 minutes to mix evenly. Other treatments are the same as $RuNiMoCrFeO_x$/CNT.

Preparation of RuO_2/CNT. First, 8.0 mg $Ru_3(CO)_{12}$ and 5.0 mg of processed MWCNT were mixed and ground in a mortar for 10 minutes to mix evenly. Other treatments are the same as $RuNiMoCrFeO_x$/CNT.

Physical and electrochemical characterizations. To study the morphology and structure of the catalyst, a scanning electron microscope (SEM) was tested on Hitachi S-4800 instrument. The transmission electron microscope (TEM) and high resolution TEM (HRTEM) of the catalyst were tested using FEI Tecnai-G2 F30 at an accelerating voltage of 300 KV, and the structure of the catalyst was further characterized. Powder X-ray diffraction (XRD) spectrum recording was performed on an X'Pert-PRO MPD diffractometer, which was run with Cu Kα radiation at 40 KV and 40 mA. X-ray photoelectron spectroscopy (XPS) analysis was performed with an Axis Supra spectrometer using a monochromatic Al Kα source at 15 mA and 14 kV. Scan analysis with an analysis area of 300×700 microns and a pass energy of 100 eV. The spectrum was calibrated by carbon 1s spectrum, and its main line was set to 284.8 eV, and then the valence state of the catalyst was analyzed using Casa XPS software. The catalyst that has been tested for stability is scraped from the working electrode by ultrasonic treatment and collected for the next step of SEM, TEM and XRD characterization.

Disperse 1 mg of the catalyst in 1 mL of a mixed solution of ethanol + ultrapure water + 5% Nafion (v: v: v=1:1:0.05), after sonication for 0.5 h, the different catalysts with the concentration of 1 mg mL^{-1} was obtained. Electrochemical measurements were carried out in a conventional three-electrode battery of a CHI760E Electrochemical Workstation (Shanghai Chenhua Instrument Corporation, China). A graphite rod

electrode was used as the counter electrode, and the reference electrode was a silver chloride electrodes (Ag/AgCl). A glassy carbon electrode (GCE, diameter: 3 mm, area: 0.07065 cm^2) was used as the working electrode. Take 10μL of the mixed slurry and drop it evenly on the surface of the GCE. After it is naturally dried, further electrochemical tests are performed. All potentials reported in this work are corrected using reversible hydrogen electrodes (RHE). In a 0.5 M H_2SO_4 solution saturated with N_2, linear sweep voltammetry (LSV) was used to test and evaluate the OER performance of the catalyst at a sweep rate of 5 mV s^{-1}. All polarization curves were corrected for 95% iR. The durability test was performed in 0.5 M H_2SO_4 solution using chronoamperometry. In addition, the LSV after 10,000 cycles of CV was measured to further evaluate the stability of the catalyst. Electrochemical impedance spectroscopy (EIS) measurement was performed at a frequency of 0.1 Hz to 100 kHz in a 0.5 M H_2SO_4 solution saturated with N_2.

Calculation of turnover frequency (TOF). Owing to the bulk nature of the catalysts, we selected an electrochemical method to obtain the TOF values of each sample. Nearly all the surface active sites were assumed to be accessible by the electrolyte, and then the TOF values could be calculated by the following equation:

$$TOF = \frac{I}{2FQ}$$

where I, n, and F are the current during linear sweep measurement, the number of active site number, and the Faraday constant, respectively. The factor 1/2 is because water electrolysis requires two electrons to evolve one hydrogen molecule from two protons. The values (n) were calculated from the CV data in the potential range from -0.2 V to +0.6 V vs RHE in 1 M phosphate buffer (pH=7.4) at a scan rate of 50 mV/s.

Since it is very difficult to assign the observed peaks to a given redox couple, the surface active sites are nearly in linear relationship with the integrated voltammetric charges (cathodic and anodic) over the CV curves. Assuming a one-electron process for both reduction and oxidation, we can evaluate the upper limit of the active site number according to the follow formula:

$$n = \frac{Q_{cv}}{2F}$$

where the Q represent the whole charge of CV curve.

Electrochemical *in situ* FTIR test. The intermediate products during the OER process were detected by in situ FTIR through Thermo iS50 FTIR with a liquid-nitrogen-cooled MCT-A detector. The in situ FTIR curves were collected by the method of internal reflection. Firstly, the catalysts modified silicon crystal plated with gold was used as working electrode, Ag/AgCl and Pt wire were worked as reference electrode and counter electrode respectively. All the tests were conducted in N_2 saturated 0.5 M H_2SO_4. The applied potential was stepped positively from 0.8 V to 1.8 V (vs. RHE) with an interval of 200 mV. Secondly, the results of in situ FTIR were reported as relative change in absorbance: $\Delta R/R = (R(ES)- R(ER))/R(ER)$. The R(ES) and R(ER) are the spectra collected at the applied potential and reference potential.

***In situ* Differential electrochemical mass spectrometry (DEMS) measurement.** We applied the Faraday scan analysis of DEMS. A mass spectrum is a two-dimensional representation of ions with the measured m/z on the x-axis and the abundance on the y-axis. First, in order to exclude the influence of impurity gases in the air, the gas bag was partially filled with air and then introduced into the capillary tube for mass spectrometric analysis tests (Figure S26a), and then the bag was removed to pass Ar for 20 minutes to exhaust

the air (Figure S26b), and the gas after OER was introduced into the same gas bag collected for analysis to detect the production of isotopic oxygen (Figure 4c).

The configuration entropy (S_{config}). The configurational entropy was calculated using the following formula.

$$S_{config} = -R\left[\left(\sum_{i=1}^{N} x_i \ln x_i\right)_{cation-site} + \left(\sum_{j=1}^{N} x_j \ln x_j\right)_{anion-site}\right]$$

where x_i and x_j represent the mole fractions of ions present in the cation- and anion-site, respectively, and R is the ideal gas constant (8.314 J mol^{-1} K^{-1}).

Example for HEOs with equimolar amount of different cations (5 cations → $x_j = 0.2$)

$S_{config} = -R\ (((0.2 \ln 0.2) + (0.2 \ln 0.2) + (0.2 \ln 0.2) + (0.2 \ln 0.2) + (0.2 \ln 0.2))_{cation\text{-}site} + (1 \ln 1)_{anion-site})$

$S_{config} = -R\ (5 * (0.2 \ln 0.2)) = 1.61R$

Similarly, the entropy values of the quaternary and ternary compounds can be calculated.

Figures

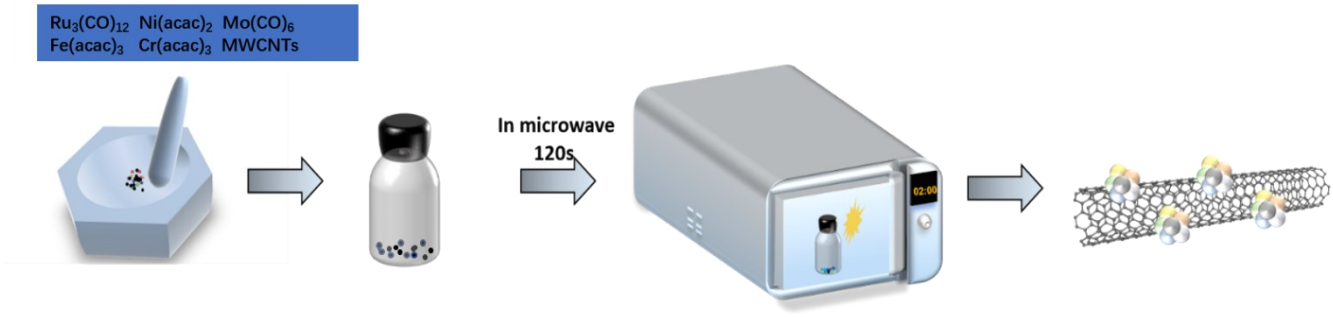

Figure S1. Schematic diagram illustrating the synthetic procedure of $RuNiMoCrFeO_x$/CNT.

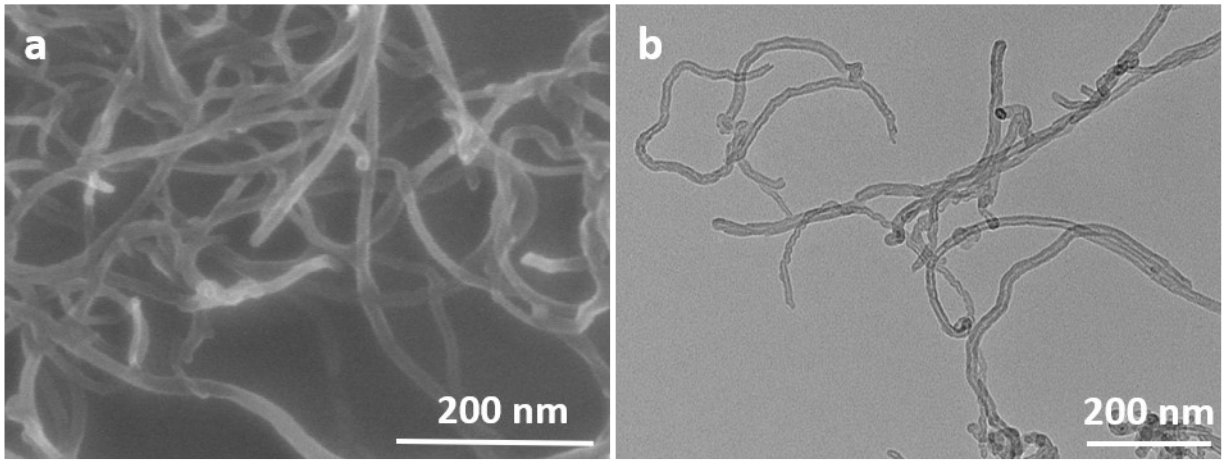

Figure S2. (a) SEM image of MWCNT. (b) TEM image of MWCNT.

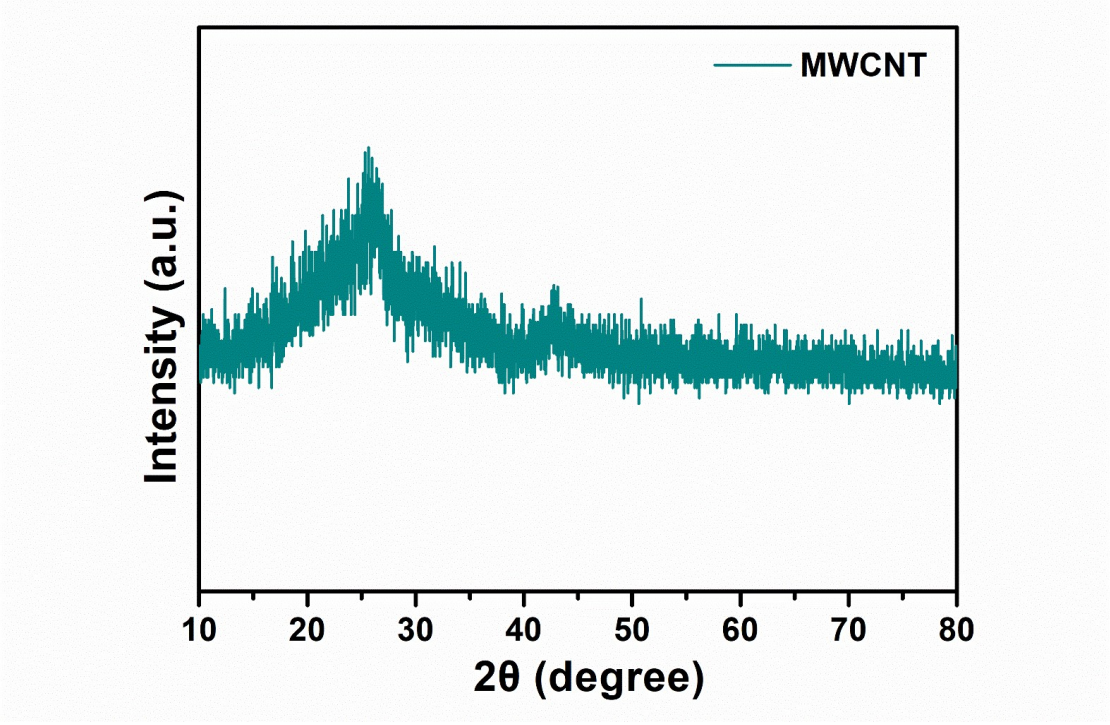

Figure S3. XRD image of MWCNT.

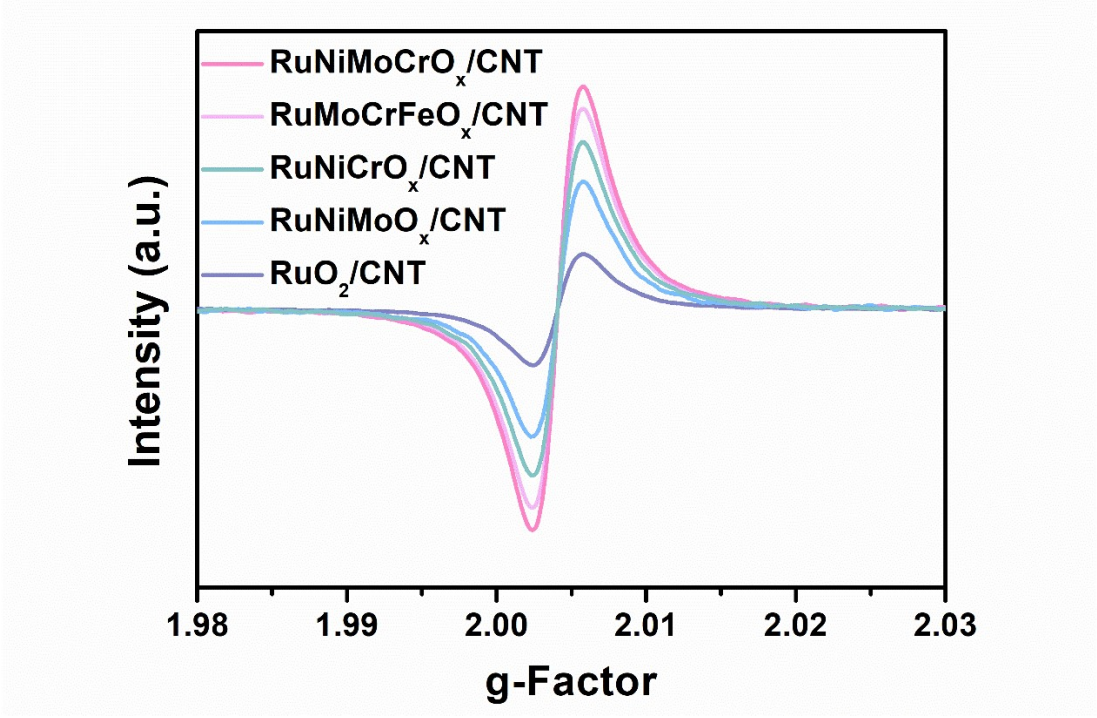

Figure S4. The ESR spectra for RuNiMoCrO$_x$/CNT, RuMoCrFeO$_x$/CNT, RuNiCrO$_x$/CNT, RuNiMoO$_x$/CNT and RuO$_2$/CNT.

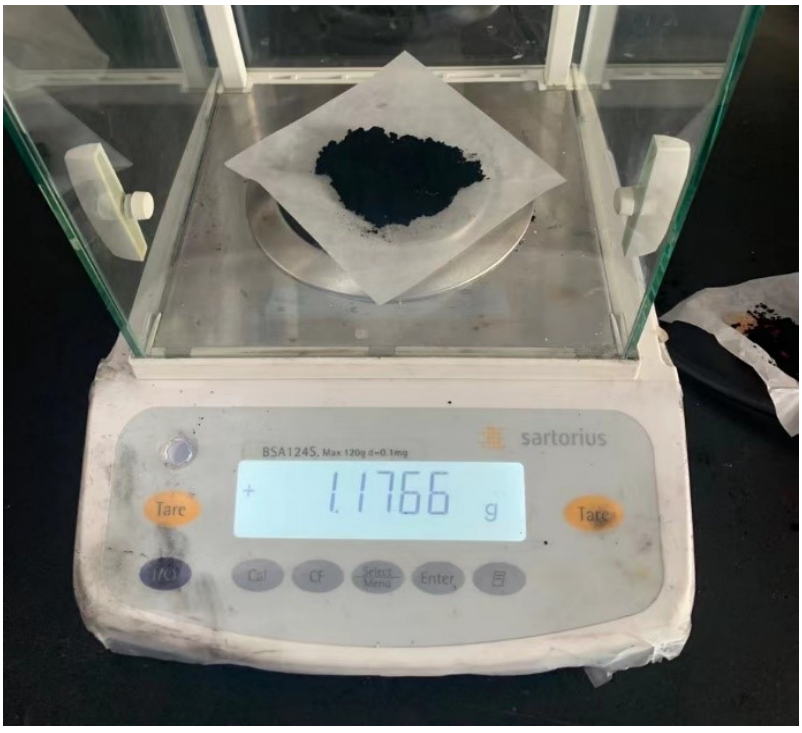

Figure S5. Image of the product after large-scale synthesis of catalyst.

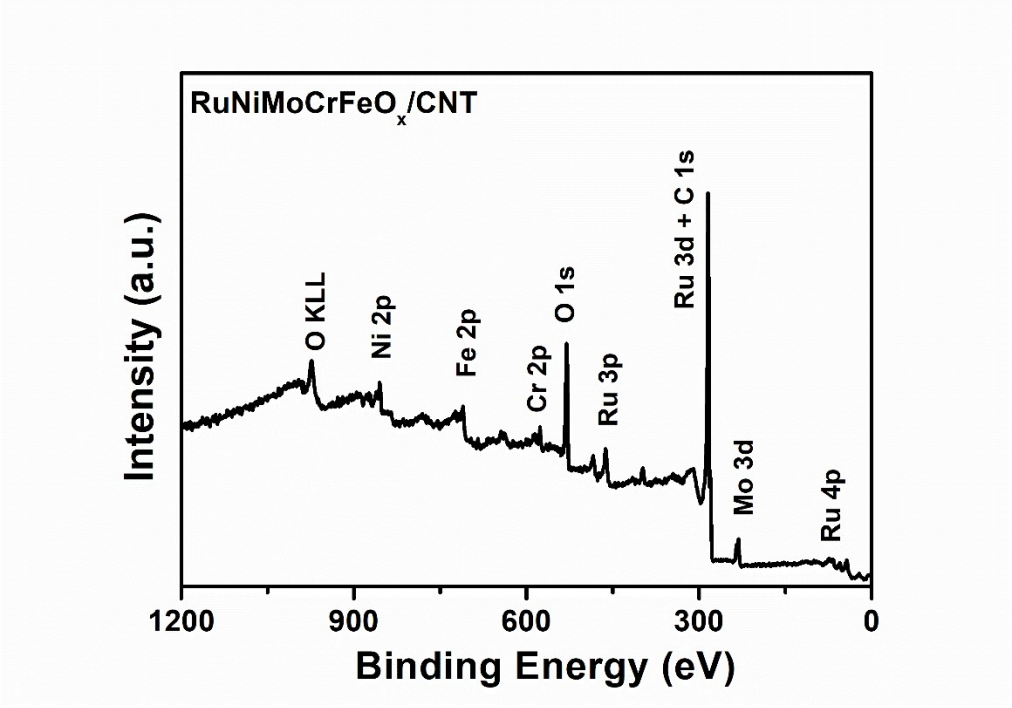

Figure S6. XPS spectra of RuNiMoCrFeO$_x$/CNT.

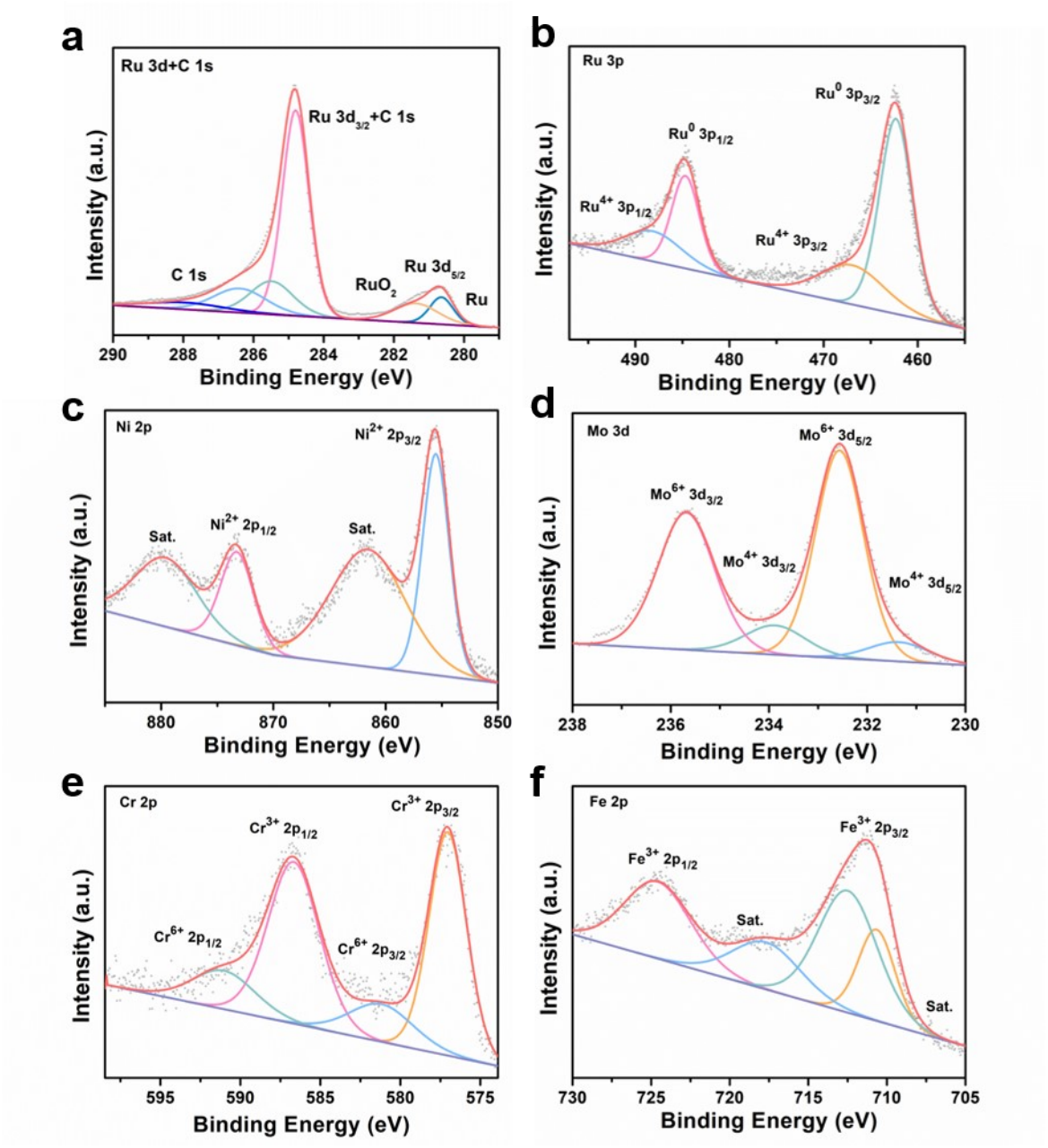

Figure S7. XPS spectra of $RuNiMoCrFeO_x$/CNT. (a) XPS spectra of Ru 3d+C 1s. (b-f) XPS spectra of Ru 3p (b) Ni 2p (c) Mo 3d (d) Cr 2p (e) and Fe 2p (f) in $RuNiMoCrFeO_x$/CNT.

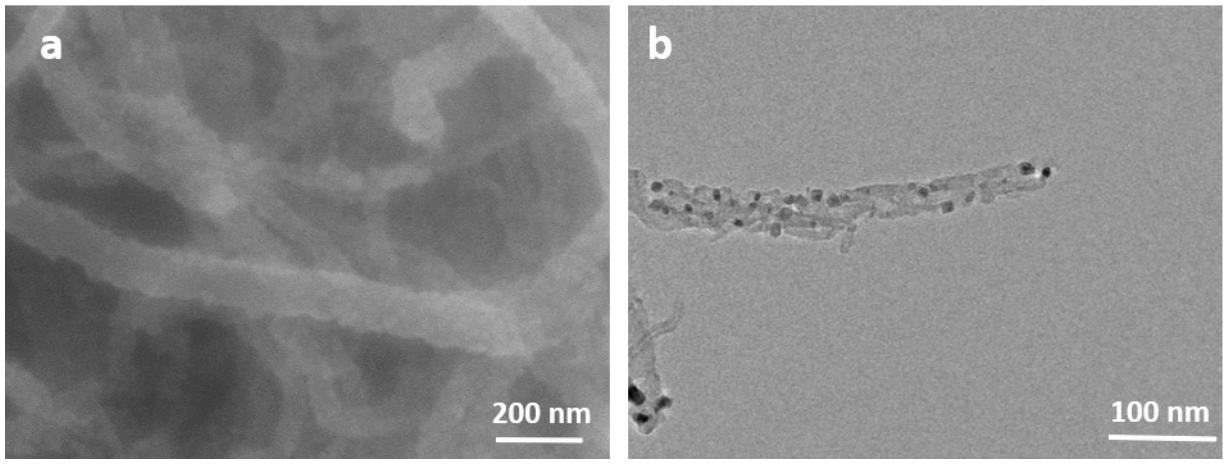

Figure S8. (a) SEM and (b) TEM images of RuO_2/CNT.

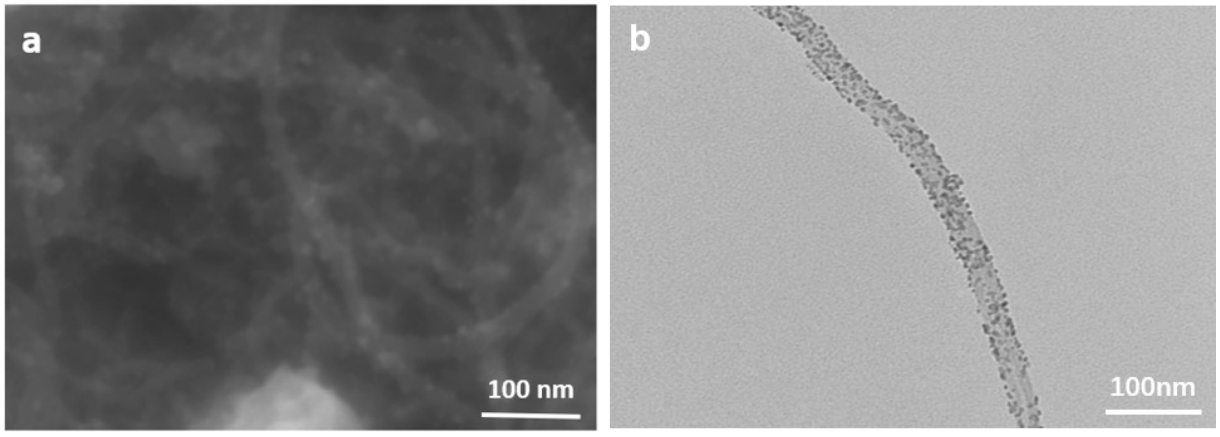

Figure S9. (a) SEM and (b) TEM images of $RuNiMoCrO_x$/CNT.

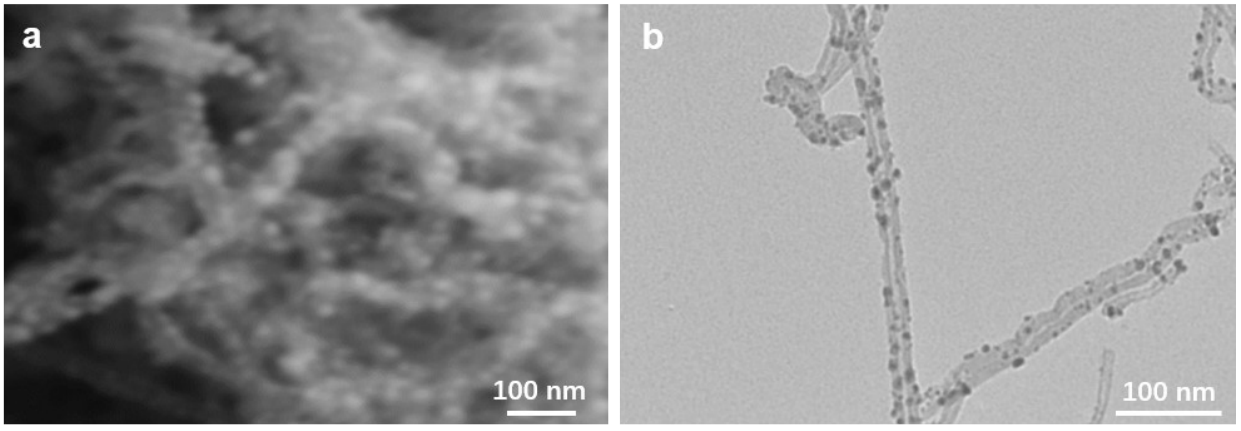

Figure S10. (a) SEM and (b) TEM images of $RuMoCrFeO_x$/CNT.

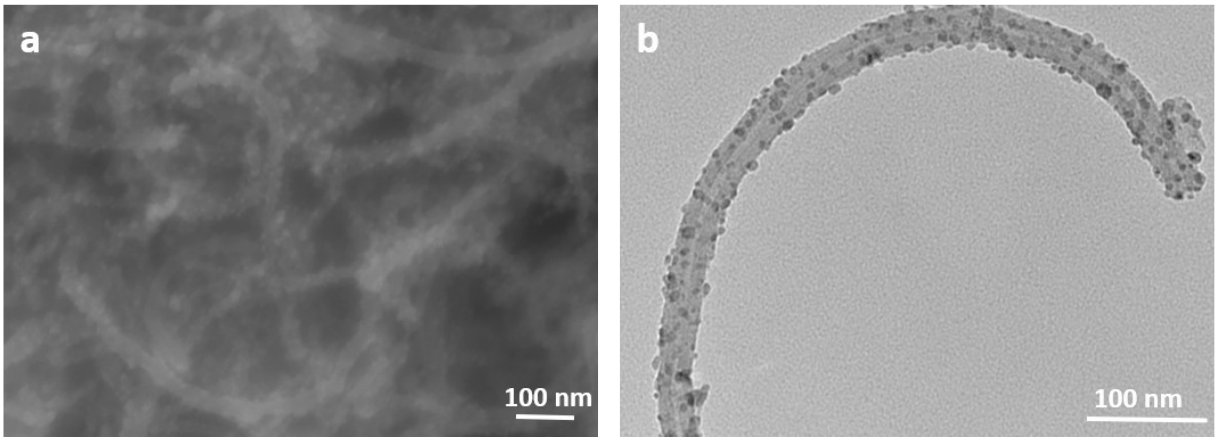

Figure S11. (a) SEM and (b) TEM images of $RuNiMoO_x$/CNT.

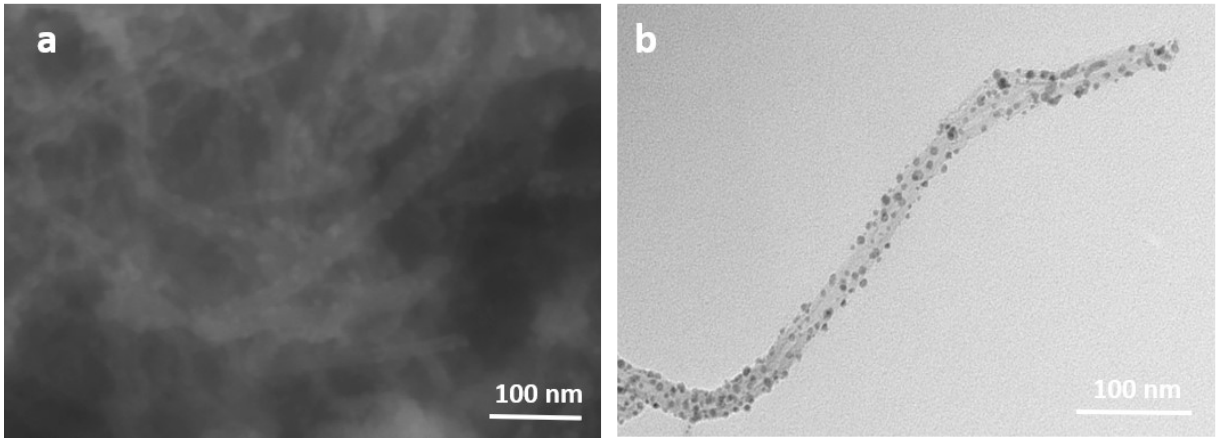

Figure S12. (a) SEM and (b) TEM images of $RuNiCrO_x$/CNT.

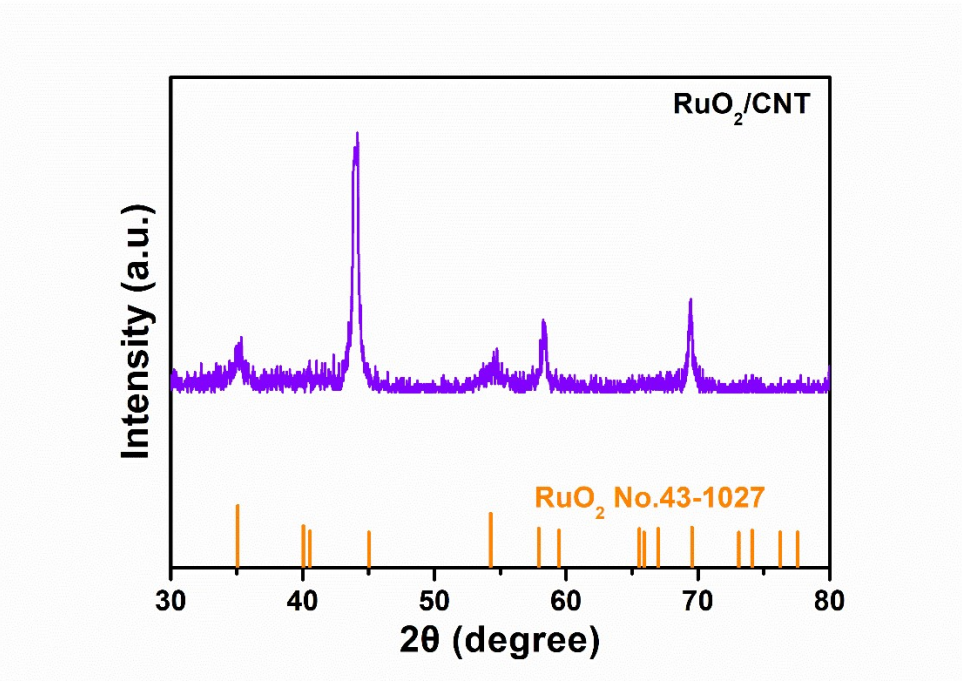

Figure S13. XRD image of RuO_2/CNT.

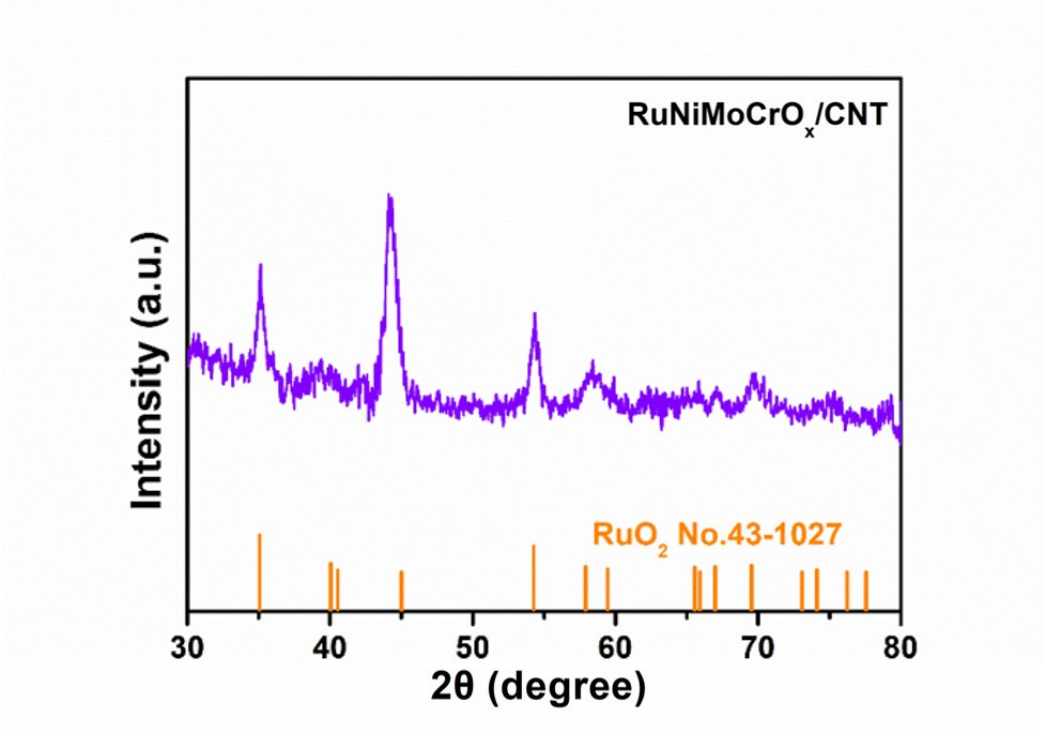

Figure S14. XRD image of $RuNiMoCrO_x$/CNT.

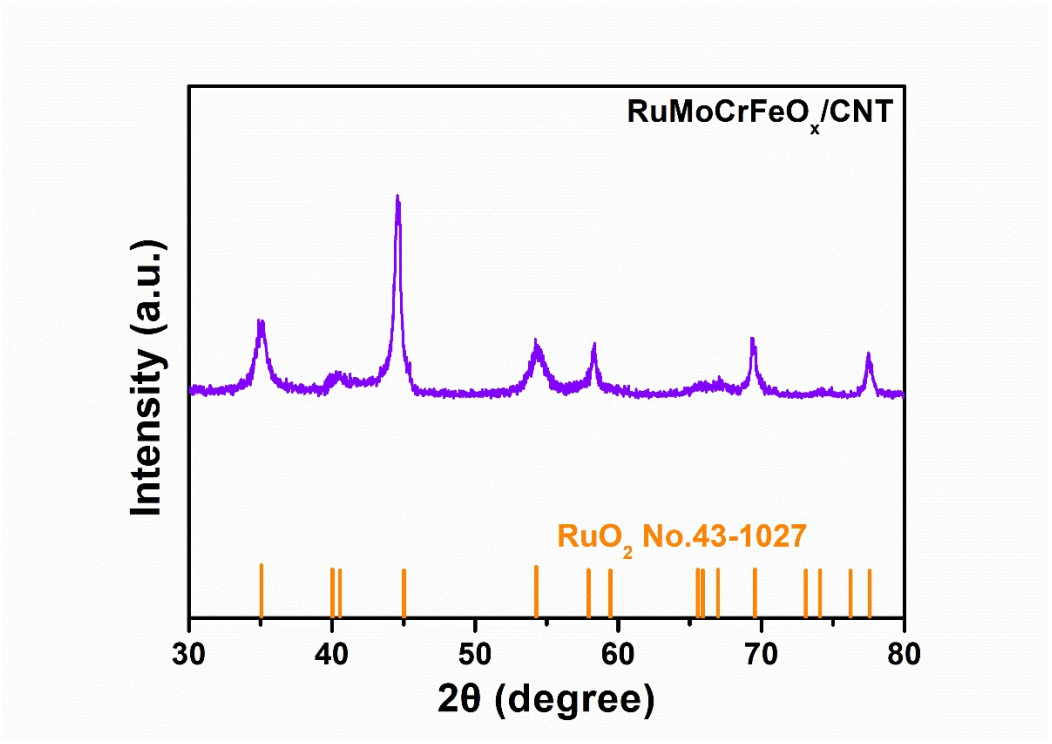

Figure S15. XRD image of RuMoCrFeO$_x$/CNT.

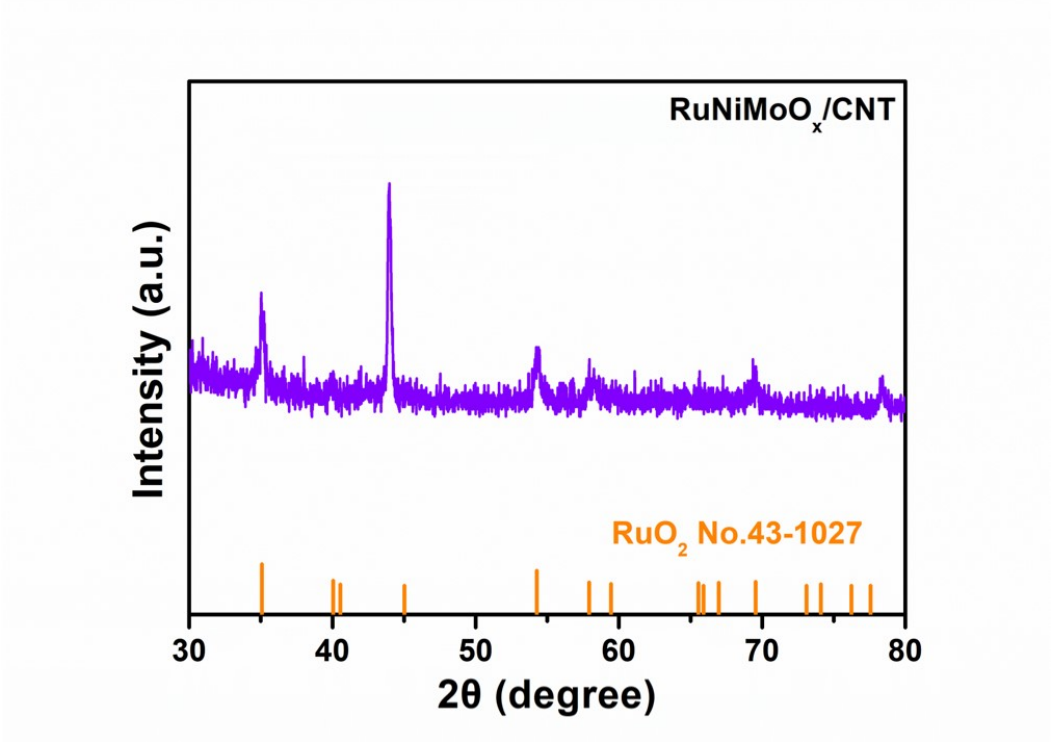

Figure S16. XRD image of RuNiMoO$_x$/CNT.

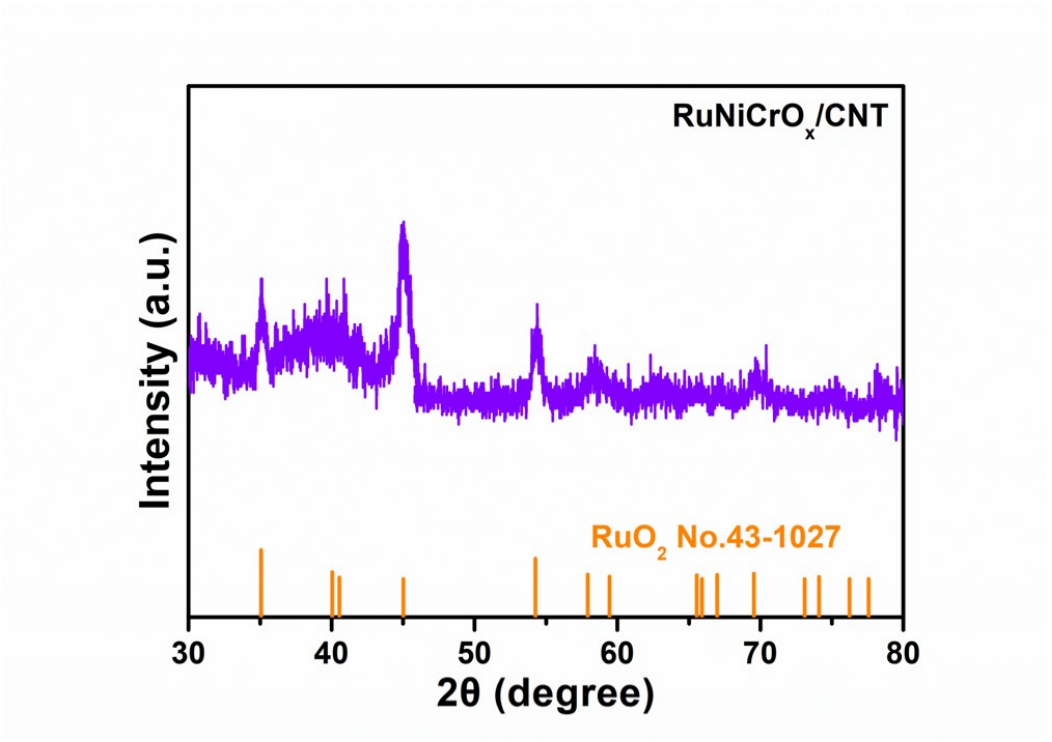

Figure S17. XRD image of RuNiCrO$_x$/CNT.

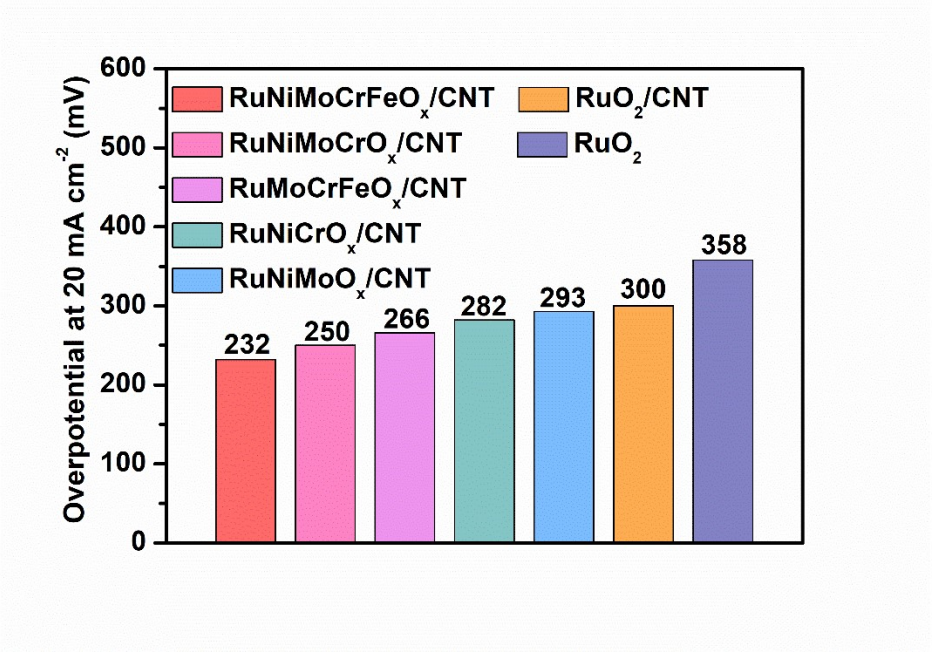

Figure S18. Comparison of overpotential at 20 mA cm^{-2} of RuNiMoCrFeO$_x$/CNT, RuNiMoCrO$_x$/CNT, RuMoCrFeO$_x$/CNT, RuNiCrO$_x$/CNT, RuNiMoO$_x$/CNT, RuO$_2$/CNT, commercial RuO$_2$ catalysts.

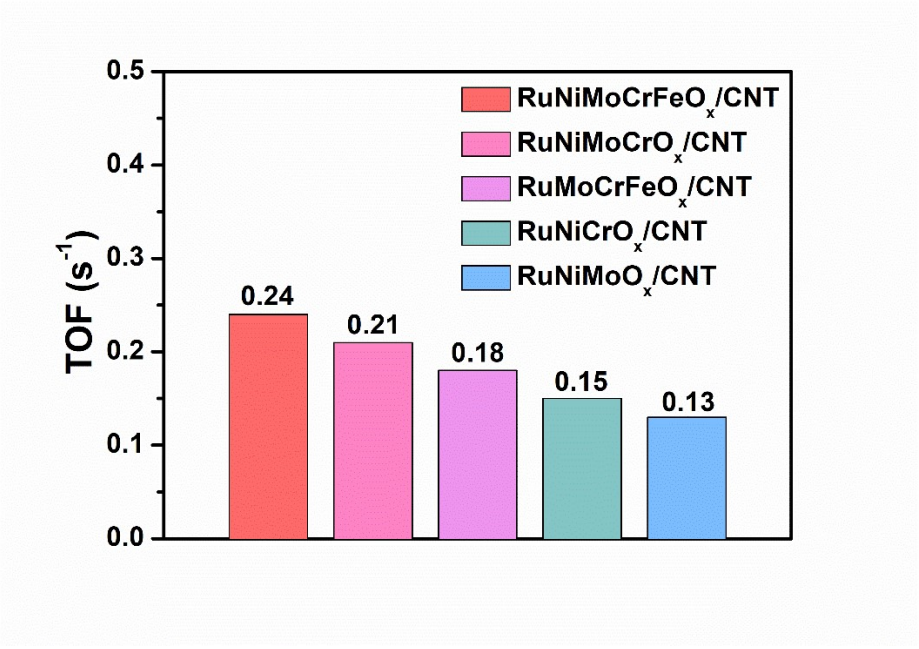

Figure S19. TOF values of RuNiMoCrFeO$_x$/CNT, RuNiMoCrO$_x$/CNT, RuMoCrFeO$_x$/CNT, RuNiCrO$_x$/CNT, RuNiMoO$_x$/CNT at the overpotential of 250 mV.

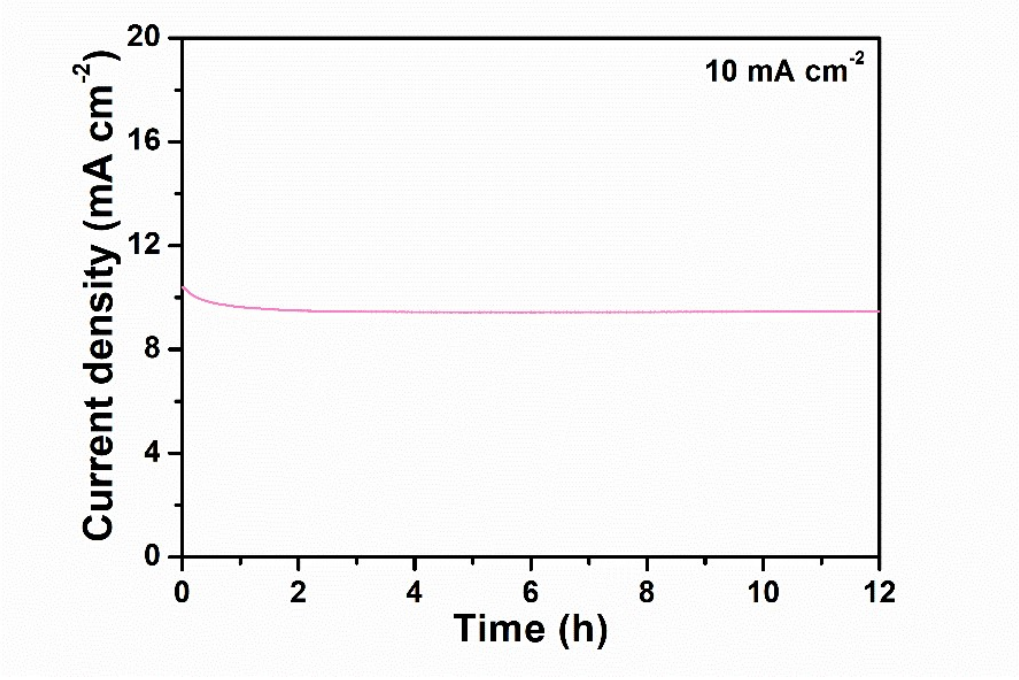

Figure S20. Chronoamperometric measurement curves of RuNiMoCrFeO$_x$/CNT catalyst for OER.

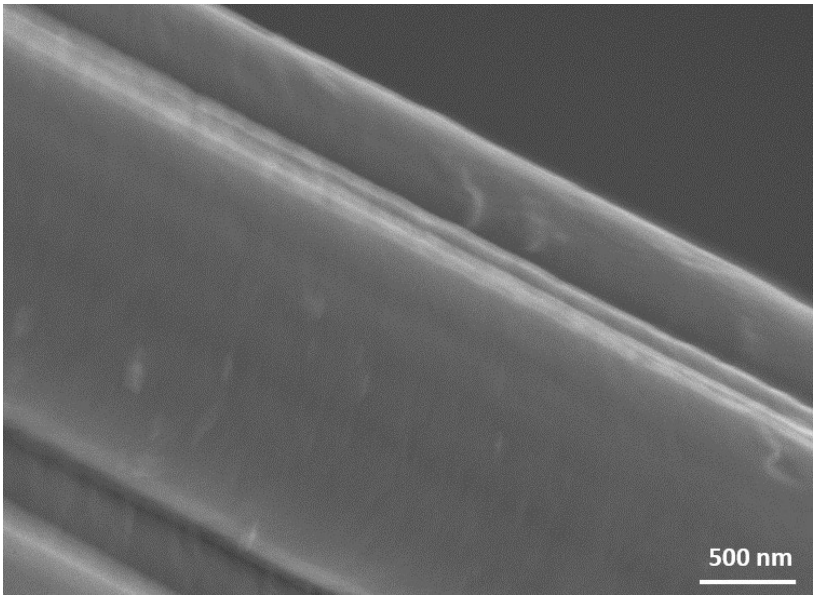

Figure S21. SEM image of pure CC.

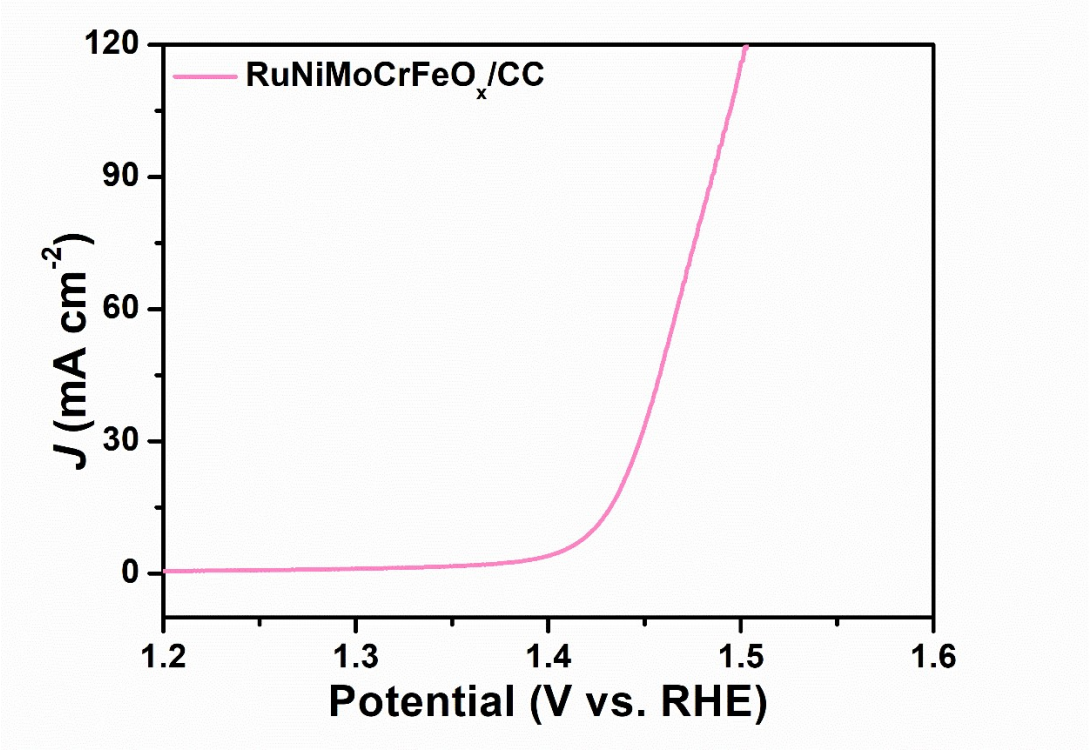

Figure S22. OER polarization curves of RuNiMoCrFeO$_x$/CC in 0.5 M H_2SO_4.

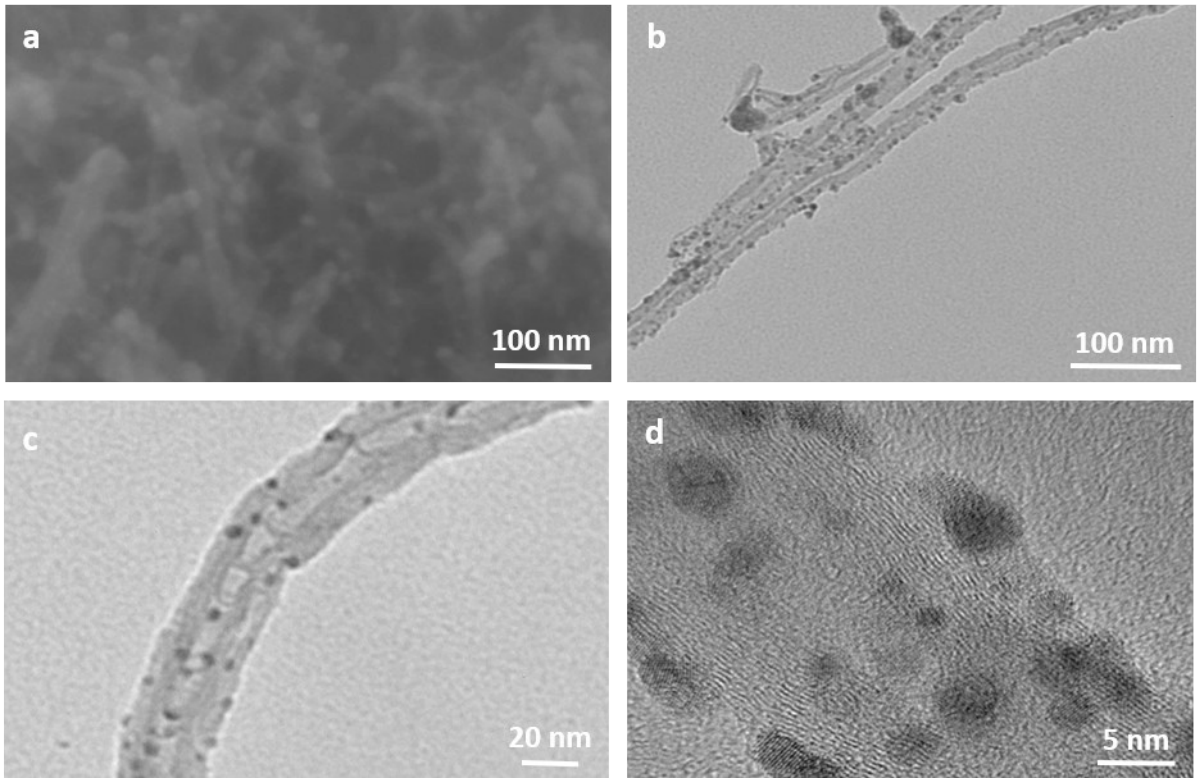

Figure S23. (a) SEM, (b, c) TEM and (d) HRTEM images of RuNiMoCrFeO$_x$/CNT after OER.

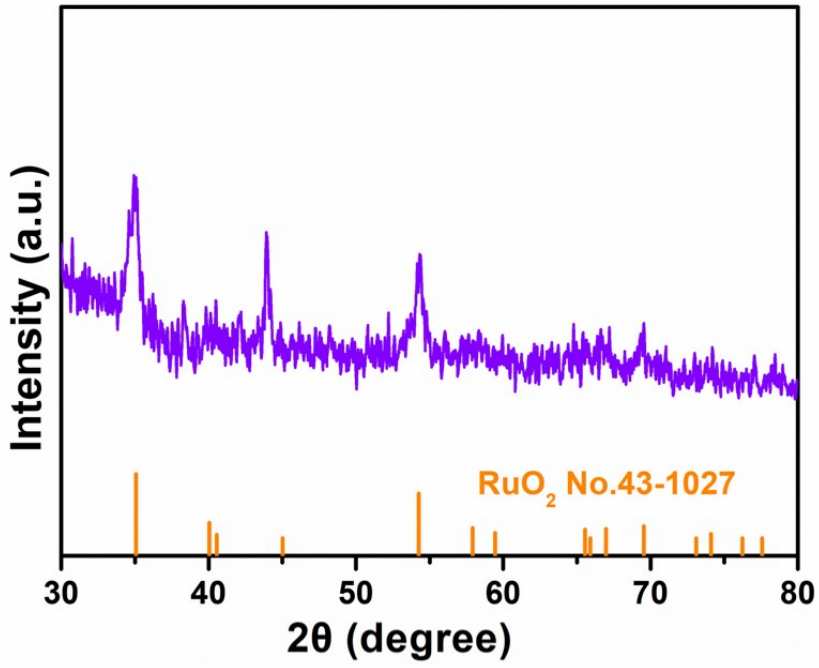

Figure S24. XRD image of RuNiMoCrFeO$_x$/CNT after OER.

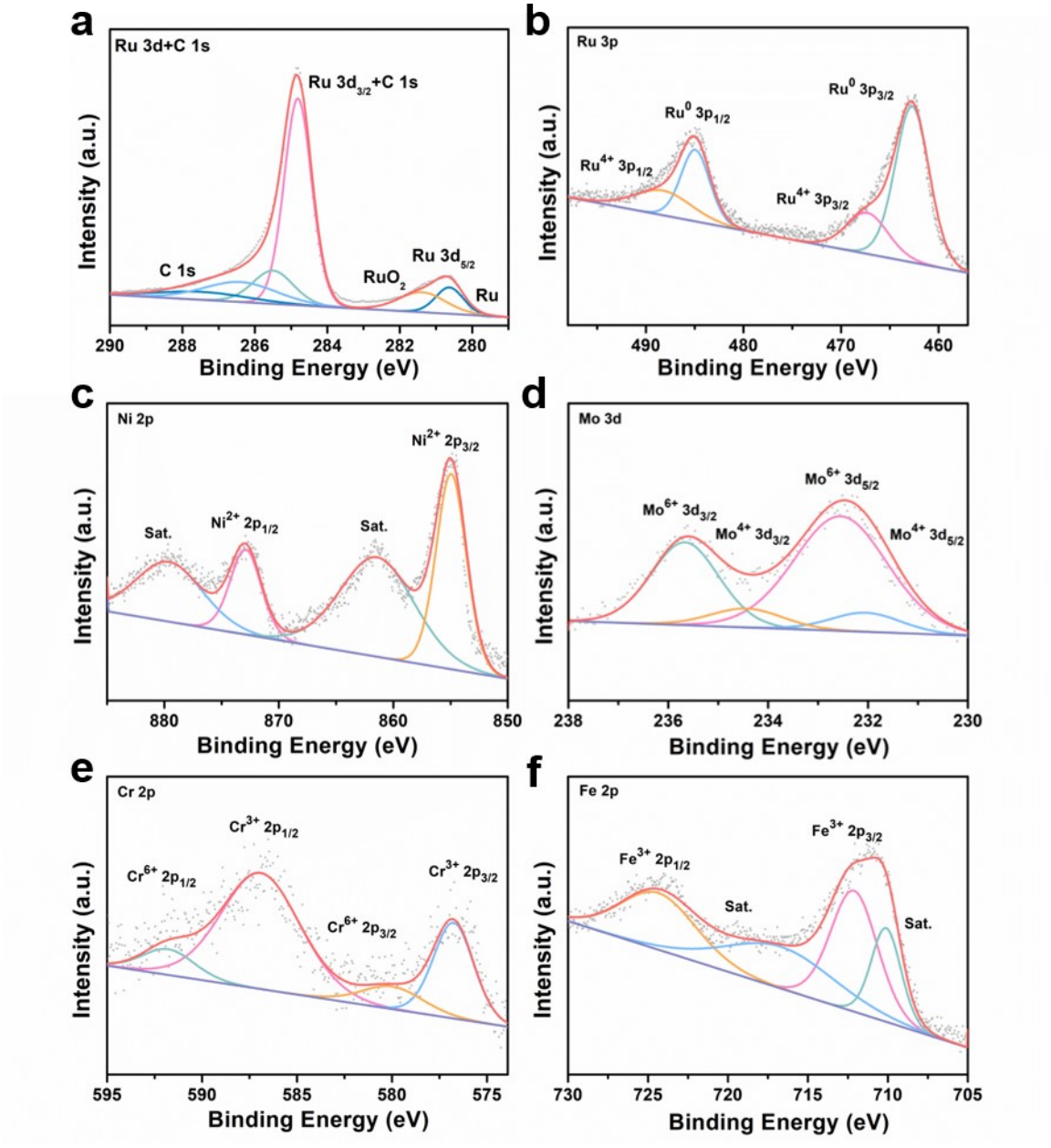

Figure S25. XPS spectra of RuNiMoCrFeO$_x$/CNT after OER. (a) XPS spectra of C 1s. (b–f) XPS spectra of Ru 3p (b), Ni 2p (c), Mo 3d (d), Cr 2p (e), and Fe 2p (f) in RuNiMoCrFeO$_x$/CNT.

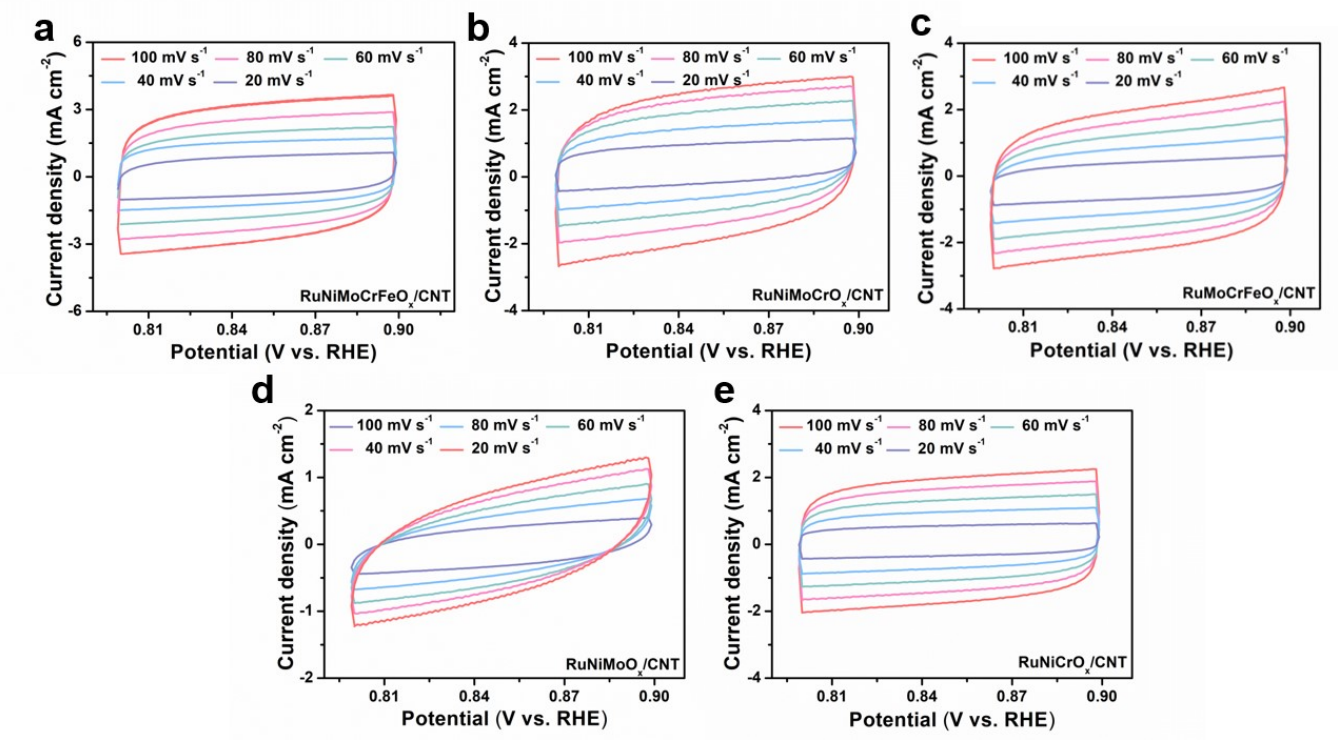

Figure S26. CV curves measured at different scan rates from 20 to 100 mV s^{-1} in 0.5 M H_2SO_4 for $RuNiMoCrFeO_x$/CNT (a), $RuNiMoCrO_x$/CNT (b), $RuMoCrFeO_x$/CNT (c), $RuNiMoO_x$/CNT (d), $RuNiCrO_x$/CNT (e).

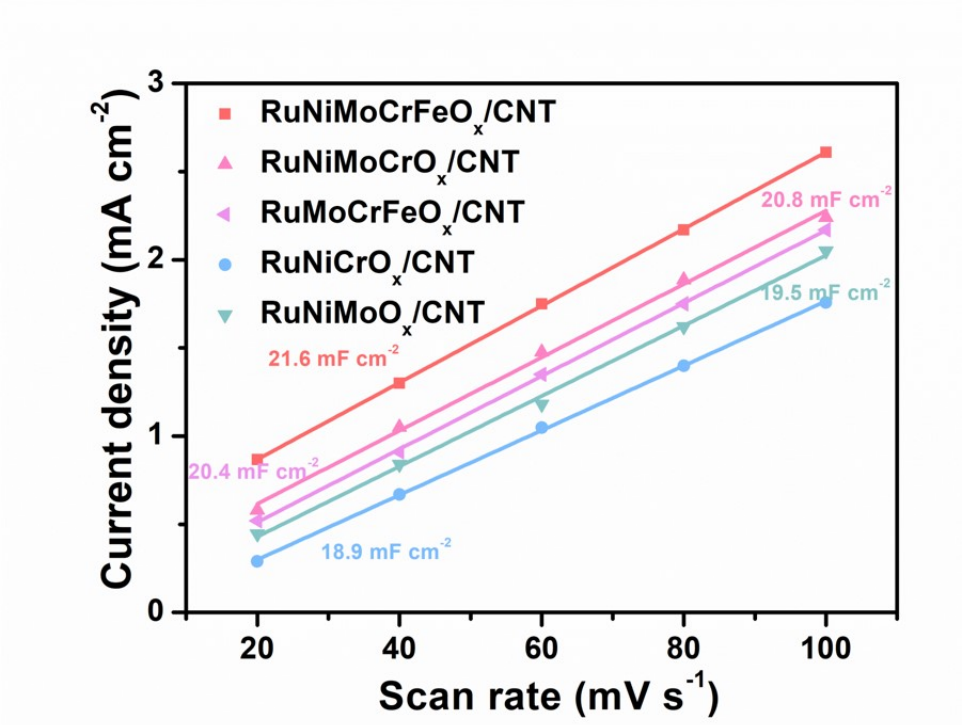

Figure S27. Capacitive current at middle potential of CV curves as function of scan rates for RuNiMoCrFeO$_x$/CNT, RuNiMoCrO$_x$/CNT, RuMoCrFeO$_x$/CNT, RuNiMoO$_x$/CNT, RuNiCrO$_x$/CNT catalysts.

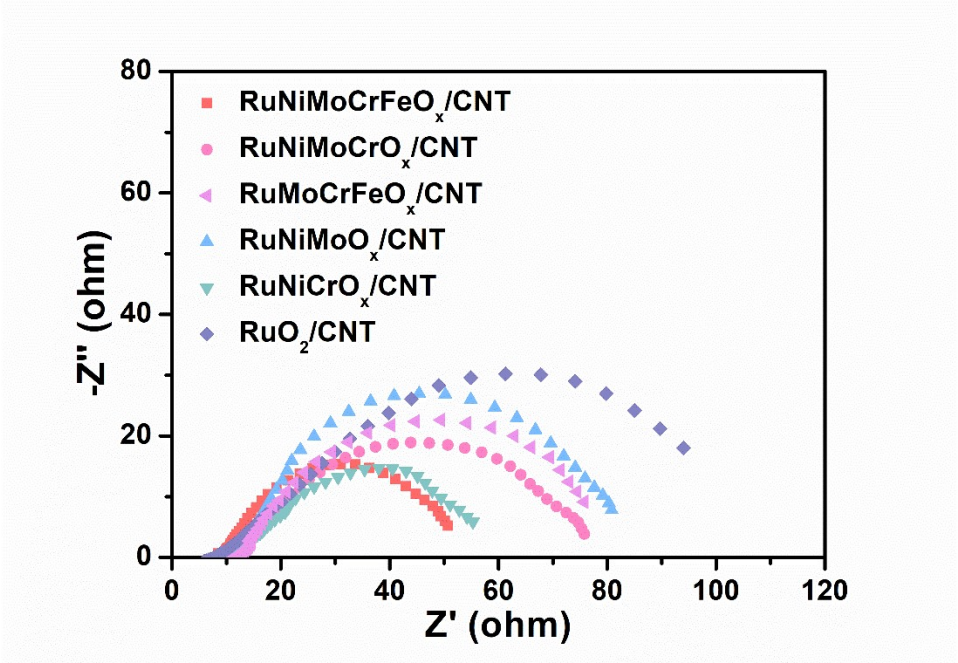

Figure S28. EIS Nyquist plots of RuNiMoCrFeO$_x$/CNT, RuNiMoCrO$_x$/CNT, RuMoCrFeO$_x$/CNT, RuNiMoO$_x$/CNT, RuNiCrO$_x$/CNT catalysts.

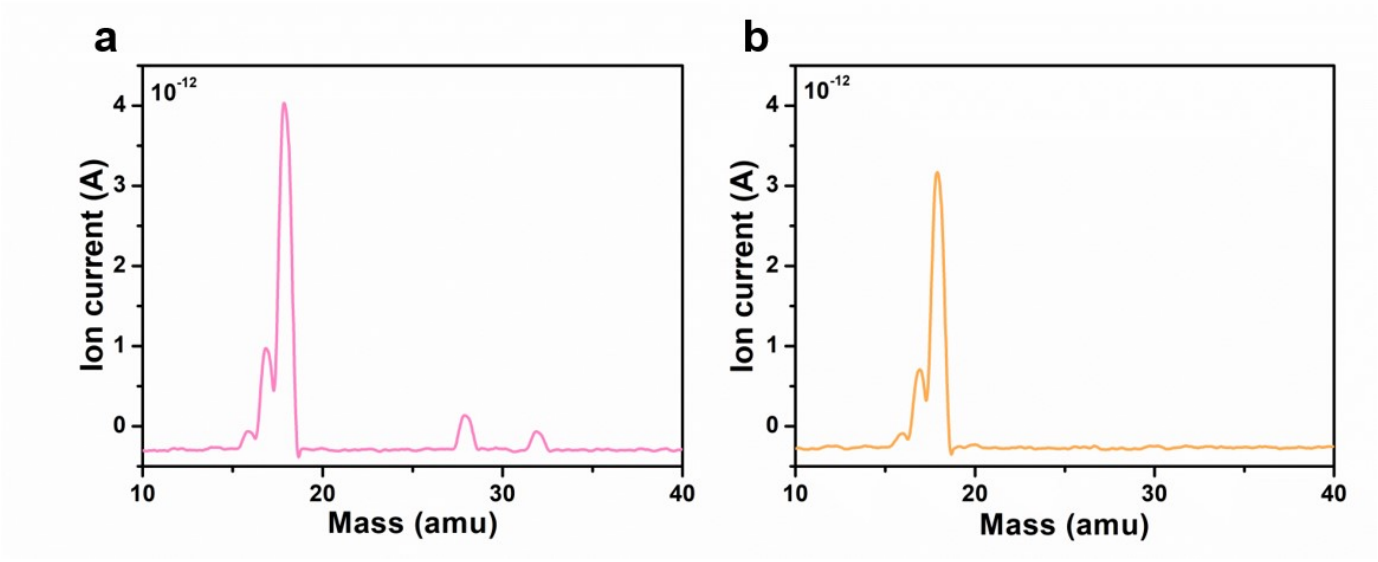

Figure S29. (a) Collected air mass spectrometry and (b) Argon mass spectrometry by DEMS.

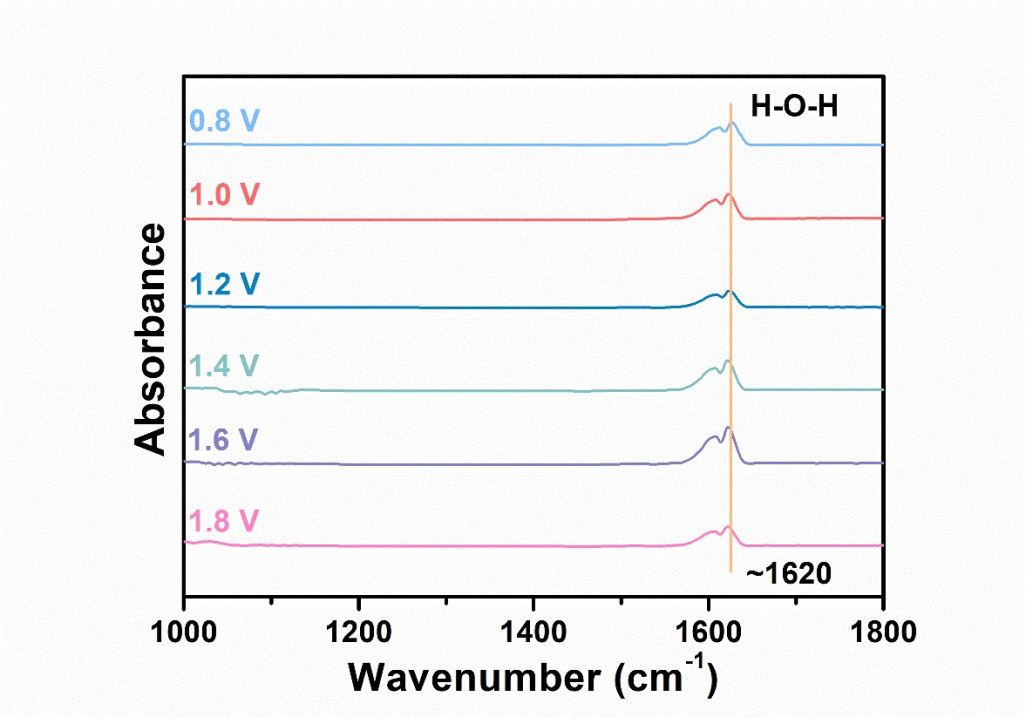

Figure S30. *In situ* FTIR spectra of $RuNiMoCrFeO_x$/CNT.

Table S1. Comparing the catalytic performance of $RuNiMoCrFeO_x$/CNT with comparison samples under acid OER catalysts.

Catalysts	Overpotential@10mV cm^{-2}	Tafel slope (mV dec^{-1})
$RuNiMoCrFeO_x$/CNT	219	47
$RuNiMoCrO_x$/CNT	240	48
$RuMoCrFeO_x$/CNT	253	50
$RuNiMoO_x$/CNT	280	61
$RuNiCrO_x$/CNT	271	60
RuO_2/CNT	280	99
Commercial RuO_2	288	195

Table S2. Comparison of TOF in this study and other recently Ru-based OER electrocatalysts in acidic solutions.

No.	Catalysts	TOF	References
1	**$RuNiMoCrFeO_x$/CNT**	**0.24 s^{-1} at 250 mV**	**This work**
2	**$RuNiMoCrO_x$/CNT**	**0.21 s^{-1} at 250 mV**	**This work**
3	**$RuMoCrFeO_x$/CNT**	**0.18 s^{-1} at 250 mV**	**This work**
4	**$RuNiMoO_x$/CNT**	**0.13 s^{-1} at 250 mV**	**This work**
5	**$RuNiCrO_x$/CNT**	**0.15 s^{-1} at 250 mV**	**This work**
6	$Ho_2Ru_2O_7$ (HRO)	0.081 s^{-1} at 300 mV	1
7	Sr−Ru−Ir ternary oxide electrocatalysts	0.13 s^{-1} at 300 mV	2
8	$Cr_{0.6}Ru_{0.4}O_2$	0.15 s^{-1} at 260 mV	3

9	Porous $Y_2[Ru_{1.6}Y_{0.4}]O_{7-\delta}$	0.055 s^{-1} at 270 mV	4
10	Cu-doped RuO_2	0.053 s^{-1} at 250 mV	5

Table S3. Summary of recently reported representative Ru-based OER electrocatalysts in acidic solutions.

No.	Catalysts	Electrolyte	Overpotential at 100 mA cm^{-2} (mV)	Durability	References
1	**RuNiMoCrFeO$_x$/CC**	**0.5M H_2SO_4**	**261**	**100 h at 100 mA cm^{-2}**	**This work**
2	C-RuO_2-RuSe	0.5M H_2SO_4	294	50 h at 10 mA cm^{-2}	6
3	Ru/RuS_2 heterostructure	0.5M H_2SO_4	319	24 h at 10 mA cm^{-2}	7

Table S4. Synthesized compounds used for electrochemical testing.

Catalysts	Entropy	Removed element
RuNiMoCrFeO$_x$/CNT	1.61 R	-
RuNiMoCrO$_x$/CNT	1.39 R	Fe
RuMoCrFeO$_x$/CNT	1.39 R	Ni
RuNiMoO$_x$/CNT	1.10 R	Cr, Fe
RuNiCrO$_x$/CNT	1.10 R	Mo, Fe

Table S5. Synthesized compounds used for electrochemical testing.

Solution	Ru	Ni	Mo	Cr	Fe
After OER	-	0.0038	0.0111	0.0095	0.0086

References

1. J. Yan, J. Zhu, D. Chen, S. Liu, X. Zhang, S. Yu, Z. Zeng, L. Jiang and F. Du, *J. Mater. Chem. A*, 2022, **10**, 9419-9426.

2. Y. Wen, P. Chen, L. Wang, S. Li, Z. Wang, J. Abed, X. Mao, Y. Min, C. Dinh, P. Luna, R. Huang, L. Zhang, L. Wang, L. Wang, R. Nielsen, H. Li, T. Zhuang, C. Ke, O. Voznyy, Y. Hu, Y. Li, W. Goddard, B. Zhang, H. Peng and E. Sargent, *J. Am. Chem. Soc.*, 2021, **143**, 6482-6490.
3. Y. Lin, Z. Tian, L. Zhang, J. Ma, Z. Jiang, B. Deibert, R. Ge and L. Chen, *Nat. Commun.*, 2019, **10**, 162.
4. J. Kim, P. Shih, Y. Qin, Z. Al-Bardan, C. Sun and H. Yang, *Angew. Chem. Int. Ed.*, 2018, **57**, 13877-13881.
5. J. Su, R. Ge, K. Jiang, Y. Dong, F. Hao, Z. Tian, G. Chen and L. Chen, *Adv. Mater.*, 2018, **30**, 1801351.
6. J. Wang, C. Cheng, Q. Yuan, H. Yang, F. Meng, Q. Zhang, L. Gu, J. Cao, L. Li, S.-C. Haw, Q. Shao, L. Zhang, T. Cheng, F. Jiao and X. Huang, *Chem*, 2022, **8**, 1673-1687.
7. J. Zhu, Y. Guo, F. Liu, H. Xu, L. Gong, W. Shi, D. Chen, P. Wang, Y. Yang, C. Zhang, J. Wu, J. Luo and S. Mu, *Angew. Chem. Int. Ed.*, 2021, **60**, 12328-12334.